ISSN 1070-3284, Russian Journal of Coordination Chemistry, 2023, Vol. 49, No. 12, pp. 830–840. © Pleiades Publishing, Ltd., 2023.
Russian Text © The Author(s), 2023, published in Koordinatsionnaya Khimiya, 2023, Vol. 49, No. 12, pp. 790–800.

Synthesis and Specific Features of the Molecular and Crystal Structures of $Cp_4Ru_4(\mu_3\text{-}CO)_4$ Cluster

S. V. Osintseva[a], O. V. Semeikin[a], F. M. Dolgushin[b, *], E. D. Tselukovskaya[c], and I. V. Anan'ev[b, c]

[a] *Nesmeyanov Institute of Organoelement Compounds, Russian Academy of Sciences, Moscow, Russia*
[b] *Kurnakov Institute of General and Inorganic Chemistry, Russian Academy of Sciences, Moscow, Russia*
[c] *National Research University Higher School of Economics, Moscow, Russia*
**e-mail: fmdolgushin@gmail.com*

Received February 14, 2023; revised February 19, 2023; accepted February 20, 2023

Abstract—Tetranuclear cluster $[Ru(\mu_3\text{-}CO)Cp]_4$ (I) is synthesized as a minor product in the thermal reaction of cyclopentadiene with $Ru_3(CO)_{12}$ aimed at preparing ruthenium dimer $[Ru(CO)_2Cp]_2$. The spectral (^{13}C and ^1H NMR, IR) and structural studies are carried out for cluster I. Under different conditions, the crystallization of cluster **I** gives dark cherry-colored crystals of two types: cluster Ia and its tetrahydrate Ib. The structures of compounds **Ia** and **Ib** are determined by X-ray diffraction (XRD) (CIF files CCDC nos. 2241197 and 2241199, respectively). A comparative analysis of the cluster geometry shows that the distortion of the $Ru_4(CO)_4$ cage in compound **I** from the ideal T_d symmetry in the structure of the pure compound is due to anisotropy of intermolecular contacts in the crystal. Specific features of chemical binding in the $[Ru(\mu_3\text{-}CO)Cp]_4$ cluster and its iron-containing analog are studied by DFT calculations using topological analysis of the electron density comparing the energy characteristics and effective force constants of binding interactions. A necessity to use criteria of elastic deformations of interatomic interactions (force constants) for the correction description of such structural chemical phenomena as structural nonrigidity of the cage in transition metal clusters is demonstrated.

Keywords: ruthenium cyclopentadienyl complexes, ruthenium carbonyl complexes, metal clusters, XRD, crystal structure, DFT calculations, electron density, metal–metal bond

DOI: 10.1134/S1070328423600249

INTRODUCTION

Binuclear complexes $[M(CO)_2Cp]_2$ (where M = Fe, Ru, and Os) are popular due to their unusual structures with many isomeric forms [1, 2], a variety of photochemical properties [3], and demand as the starting reagents for the synthesis of the cyclopentadienyl derivatives [4, 5]. Our study also started from the synthesis of $[Ru(CO)_2Cp]_2$ as the initial compound, but interest in the chemistry of the polynuclear ruthenium complexes [6, 7] enforced us to consider the synthesis of this dimer in more detail.

The procedure for the preparation of ruthenium dimer $[Ru(CO)_2Cp]_2$ by the thermal reaction of cyclopentadiene with $Ru_3(CO)_{12}$ has been described 50 years ago [8] and further was multiply modified [9–11]. The mononuclear hydride complex $HRu(CO)_2Cp$ and dimer $[Ru(CO)_2Cp]_2$ are mentioned as reaction products in the literature. However, it is known that drastic conditions of the reaction result in the formation of the complexes with different nuclearities [12]. Taking into account specific features of the $[Ru(CO)_2Cp]_2$ dimer existing in a solution at room temperature as four isomers [2], we can expect a multicomponent mixture in the reaction, the composition of which is much richer than a habitual set of isolated products.

In this article, we describe minor products of the thermal reaction of cyclopentadiene with $Ru_3(CO)_{12}$, the synthesis of the tetranuclear cluster $[Ru(\mu_3\text{-}CO)Cp]_4$ (**I**) and results of its structural study, and comparative analysis of the chemical binding in cluster **I** and its iron analog according to the DFT calculation data.

EXPERIMENTAL

^1H and ^{13}C NMR spectra were recorded on an Avance-600 spectrometer (600.22 and 150.93 MHz, respectively) in a $CDCl_3$ solution using residual signals of incompletely deuterated $CDCl_3$ (for $CHCl_3$, δ_H = 7.25 ppm) as an internal standard. IR spectra were recorded on a Specord M80 spectrophotometer (Carl Zeiss).

Synthesis of $[Ru(\mu_3\text{-}CO)Cp]_4$ (I). An excess of freshly distilled cyclopentadiene (1 mL) and $Ru_3(CO)_{12}$ (0.5 g, 0.78 mmol) in heptane (150 mL)

were refluxed for 2.5 h. The IR spectrum of the formed light yellow solution indicated the complete conversion of $Ru_3(CO)_{12}$ to $HRu(CO)_2Cp$ [8, 13].

Air was passed overnight through the formed reaction mixture. The IR spectrum of the resulting brown mixture showed that the hydride transformed into the $[Ru(CO)_2Cp]_2$ dimer [14]. The reaction mixture was evaporated, the residue was dissolved in a small amount of dichloromethane, and the solution was chromatographed on a 20-cm column packed with silica gel (Sigma-Aldrich 2271-96). The yellow band containing ruthenocene $RuCp_2$ (5 mg, <1%) (according to the ^1H NMR spectrum [15]) was isolated by elution with petroleum ether. A substance with three M–CO bands in the IR spectrum (2002 s, 1948 s, 1920 s) was isolated from the next yellow fraction, which is presumably a dimer in the form of bridge-free carbonyl groups [14]. The subsequent elution with petroleum ether washed down a cyclopentadiene excess and products of its transformations. The further elution with a mixture of dichloromethane and petroleum ether (2 : 3) gave a yellow band of dimer $[Ru(CO)_2Cp]_2$ (208 mg, 48.2%) and an orange band containing $Ru(CO)_2CpCl$ (according to the IR spectrum [16]).

A cherry-colored band containing $[Ru(\mu_3\text{-}CO)Cp]_4$ (**I**) (5 mg, <1%) was isolated by the further elution with a mixture of acetone and petroleum ether (1 : 8).

^1H NMR ($CDCl_3$; δ, ppm): 5.22 s (C_5H_5). ^{13}C NMR ($CDCl_3$; δ, ppm): 97.2 s (C_5H_5), 248.7 s (μ_3-CO). IR (CH_2Cl_2; ν, cm^{-1}): 1638 m ν(C=O) [17, 18].

Prismatic cherry-colored crystals of compound **Ia** with yellow-colored decomposition traces at the upper boundary of the solution (presumably $Ru(CO)_2CpCl$) were obtained by the recrystallization of the cherry substance from a mixture of dichloromethane and hexane. The repeated recrystallization of the cherry substance from a mixture of acetone and hexane gave a minor amount of needle-like cherry crystals of tetrahydrate $[Ru(\mu_3\text{-}CO)Cp]_4{\cdot}4(H_2O)$ (**Ib**).

XRD for single crystals of compounds **Ia** and **Ib** was carried out on a Bruker SMART diffractometer equipped with an Apex II CCD detector (MoK_α, λ = 0.71073 Å, graphite monochromator, ω scan mode). A semiempirical absorption correction was applied using the SADABS program [19] during experimental data processing. The structures were solved by direct methods and refined by full-matrix least squares for F^2 in the anisotropic approximation for all non-hydrogen atoms. The hydrogen atoms of the water molecule in the structure of compound **Ib** were localized from the difference electron density maps and included into refinement by the riding model with $U_{iso}(H) = 1.5U_{eq}(O)$. The hydrogen atoms in the Cp ligands were placed in the calculated positions and refined by the riding model with $U_{iso}(H) = 1.2U_{eq}(C)$. The calculations were performed using the SHELXL software [20]. The crystallographic characteristics and structure refinement parameters for compounds **Ia** and **Ib** are listed in Table 1.

The full sets of XRD parameters for crystals of compounds **Ia** and **Ib** were deposited with the Cambridge Crystallographic Data Centre (CIF files CCDC nos. 2241197 and 2241199, respectively; deposit@ccdc.cam.ac.uk; http://www.ccdc.cam.ac.uk).

Theoretical calculation details. Quantum-chemical calculations were performed by the density functional theory (DFT) in the Gaussian09 program [21] using the PBE0 hybrid functional [22] and standard def2TZVP basis set [23]. Grimme's D3 empirical correction [24] with the Becke–Johnson damping [25] was applied to take into account dispersion interactions. Geometry optimization was performed using tight convergence criteria for forces on atoms and their shifts (root-mean-square for forces not higher than 10^{-5} au). An ultrafine integration grid (99 radial shells and 590 angular points) was used in energy calculations. The second derivatives of the electronic energy were calculated at the same approximation level for the optimized structures from the atomic nuclei shifts: the both systems correspond to a minimum on the corresponding potential energy surface. A topological analysis of the electron density function including the search for critical points and interatomic surfaces was performed in the AIMAll program [26]. The number of critical points of different types for both systems obeys the Poincaré–Hopf relation.

RESULTS AND DISCUSSION

Dimer $[Ru(CO)_2Cp]_2$ was synthesized from cyclopentadiene and $Ru_3(CO)_{12}$ using a standard procedure of reflux in hexane [8]. Thorough chromatography made it possible to isolate earlier nonisolated mononuclear ruthenocene $RuCp_2$ and tetranuclear complex $[Ru(\mu_3\text{-}CO)Cp]_4$ (**I**), as well as several unidentified products, along with standard mononuclear hydride complex $HRu(CO)_2Cp$ and dimer $[Ru(CO)_2Cp]_2$. Note that tetranuclear complex **I** is unstable in chlorine-containing solvents and, hence, probably was not obtained when using standard chromatography.

Cluster $[Ru(\mu_3\text{-}CO)Cp]_4$ was earlier prepared by reflux of $[Ru(CO)_2Cp]_2$ in xylene for 4 weeks. The yield was 3.4% [17]. Interestingly, a similar reaction of a mixture of $[Ru(CO)_2Cp]_2$ and $[Fe(CO)_2Cp]_2$ was carried out to prepare a heteronuclear product. No heteronuclear cluster is formed under these conditions, but the yield of $[Ru(\mu_3\text{-}CO)Cp]_4$ increases nearly two times to 6% [17]. Under UV irradiation, dimer $[Ru(CO)_2Cp]_2$ cleaves along the Ru–Ru bond to form mononuclear radicals, and further chain polynuclear complexes are formed [27]. With increasing reaction temperature (decalin, 190°C), complex

Table 1. Crystallographic characteristics and structure refinement parameters for compounds **Ia** and **Ib**

Parameter	Value	
	Ia	**Ib**
Empirical formula	$C_{24}H_{20}O_4Ru_4$	$C_{24}H_{20}O_4Ru_4 \cdot 4H_2O$
FW	776.68	848.74
T, K	120(2)	120(2)
Crystal system	Monoclinic	Tetragonal
Space group	*C*2/*c*	$I4_1/a$
a, Å	17.5226(11)	17.435(5)
b, Å	8.0635(5)	17.435(5)
c, Å	16.0441(16)	8.064(2)
β, deg	116.7065(12)	90
V, Å^3	2025.1(3)	2451.3(17)
Z	4	4
ρ_{calc}, g cm^3	2.547	2.300
μ, cm^{-1}	29.59	24.66
$2\theta_{max}$, deg	56.0	50.0
T_{min}/T_{max}	0.757/0.891	0.683/0.952
Number of measured reflections	11416	8119
Number of independent reflections	2448	1084
Number of observed reflections with $I > 2\sigma(I)$	1930	693
Number of refined parameters	145	82
GOOF	0.974	0.996
R_1 (for *F* for reflections with $I > 2\sigma(I)$)	0.0289	0.0423
wR_2 (for F^2 for all reflections)	0.0602	0.0868
Residual electron density (max/min), e Å^{-3}	0.800/–0.652	0.732/–0.845

$[Ru(\mu_3\text{-}CO)Cp]_4$ was synthesized in a 14% yield and pentanuclear complex $Ru_5(CO)_3(\mu_3\text{-}CO)_4Cp_4$ was isolated [18]. Separately conducted reactions of $[Ru(\mu_3\text{-}CO)Cp]_4$ transformation do not give complexes of higher nuclearity, and no change of μ_3-CO by μ_3-$Ru(CO)_3$ occurs. No crystals of the complexes or their phosphine derivatives suitable for XRD were obtained [18].

The standard synthesis of dimer $[Ru(CO)_2Cp]_2$ is carried out at a lower temperature (heptane, 98°C) and, hence, complex $[Ru(\mu_3\text{-}CO)Cp]_4$ was obtained in a smaller amount than that described earlier [18]. Nevertheless, we succeeded to obtain crystals of cluster **I** of rather high quality and to determine its structure.

Crystallization under different conditions (see Experimental) gave dark cherry crystals of two types: prismatic crystals of cluster **Ia** and fine needle-like crystals of tetrahydrate **Ib**.

In a crystal of compound **Ia** (monoclinic crystal system, space group *C*2/*c*), tetranuclear cluster $[Ru(\mu_3\text{-}CO)Cp]_4$ occupies a special position on twofold rotation axis passing through the centers of opposite Ru(1)–Ru(1A) and Ru(2)–Ru(2A) edges (Fig. 1). Four ruthenium atoms are arranged at the vertices of an almost regular tetrahedron in which three pairs of opposite edges have insignificantly different lengths of 2.687, 2.723, and 2.737 Å (Table 2). The μ_3-bridging carbonyl ligand with nonequivalent Ru–C(CO) distances lies above each triangular face, and two of these distances (average 2.12 Å) are somewhat longer than the third one (average 2.07 Å). All Ru–C(Cp) distances fall in a narrow range of 2.228(4)–2.258(4) Å (average 2.238 Å).

Although the mentioned deviations of the geometry of the $Ru_4(CO)_4$ cage from the ideal T_d symmetry in the structure of compound **Ia** are small by absolute value, they appreciably exceed determination inaccuracies of bond lengths and are systematic. Note that the difference in chemically equivalent bond lengths does not exceed 0.02 Å in the structure of analogous tetrahedral iron cluster $[Fe(\mu_3\text{-}CO)Cp]_4$ [28]. The

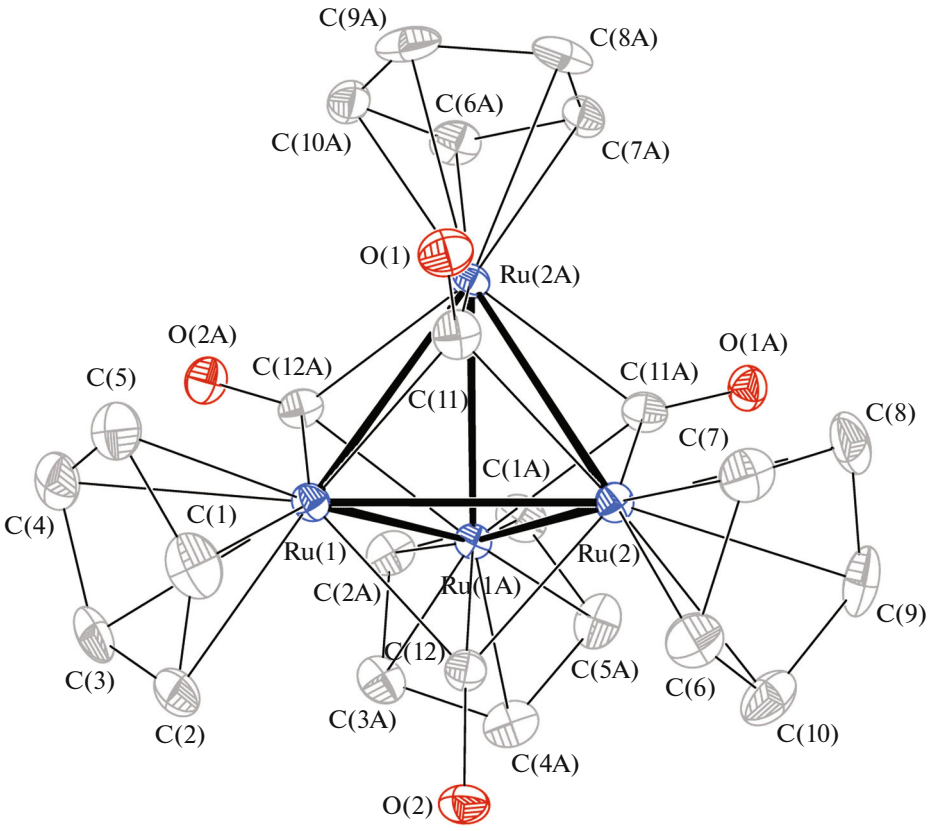

Fig. 1. Structure of cluster $[Ru(\mu_3\text{-}CO)Cp]_4$ in the crystal of **Ia** (thermal ellipsoids are given with 50% probability, and hydrogen atoms are omitted).

number of valence electrons (60e) in tetrahedral clusters **I** and its iron-containing analog are formally consistent with six metal–metal bonds and filled 18e shell for each metal atom. Therefore, causes for the distortion of the symmetric structure of cluster **I** in the absence of nonspecific intermolecular interactions in

Table 2. Bond length in cluster $[Ru(\mu_3\text{-}CO)Cp]_4$ for structures **Ia** and **Ib***

Structure **Ia**			
Ru(1)–Ru(2)	2.6872(5)	Ru(1)–Ru(2A)[a]	2.7369(5)
Ru(1)–Ru(1A)[a]	2.7213(7)	Ru(2)–Ru(2A)[a]	2.7244(7)
Ru(1)–C(11)	2.114(4)	Ru(2)–C(11)	2.121(4)
Ru(1)–C(12)	2.117(4)	Ru(2)–C(12)	2.118(4)
Ru(1)–C(12A)[a]	2.074(4)	Ru(2)–C(11A)[a]	2.068(4)
$Ru(1)–C_{Cp}$	2.231(4)–2.241(4)	O(1)–C(11)	1.219(5)
$Ru(2)–C_{Cp}$	2.228(4)–2.258(4)	O(2)–C(12)	1.202(5)
Structure **Ib**			
Ru(1)–Ru(1A)[b]	2.7185(16)	Ru(1)–C(1)	2.083(9)
Ru(1)–Ru(1B)[c]	2.7106(13)	Ru(1)–C(1A)[b]	2.097(8)
$Ru(1)–C_{Cp}$	2.220(8)–2.232(9)	Ru(1)–C(1B)[c]	2.112(9)
O(1)–C(1)	1.211(9)		

* Symmetrically equivalent atoms were revealed by the transforms: [a] $-x, y, -z + 1/2$; [b] $-x + 1, -y + 3/2, z$; [c] $y - 1/4, -x + 5/4, -z + 5/4$.

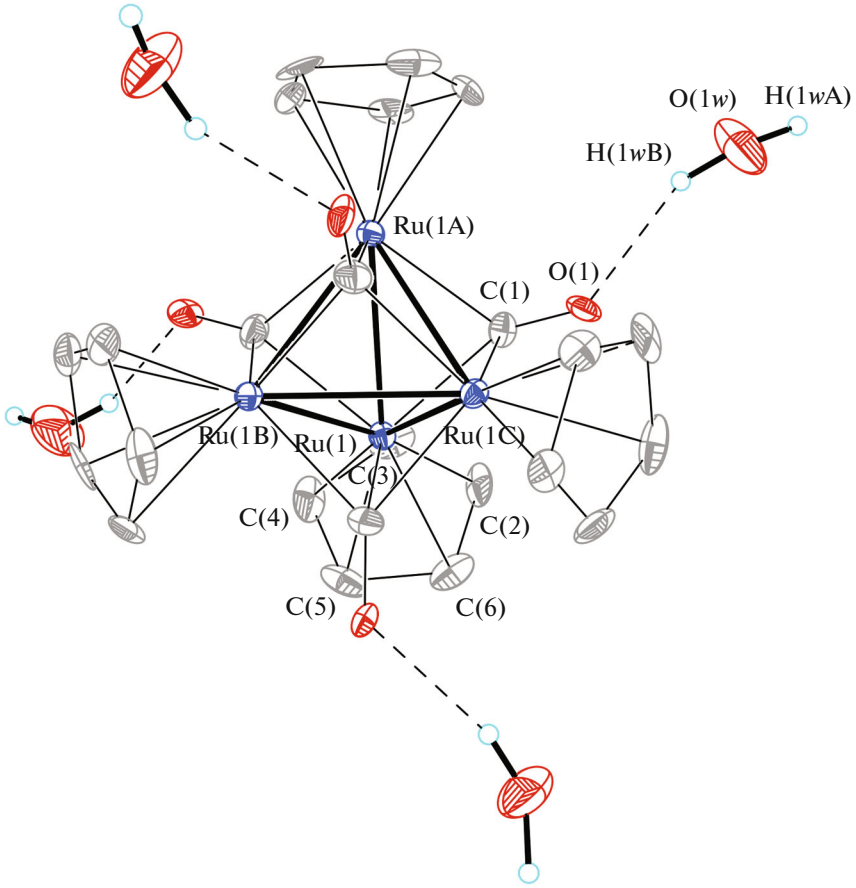

Fig. 2. Structure of tetrahydrate $[Ru(\mu_3\text{-}CO)Cp]_4 \cdot 4(H_2O)$ in the crystal of **Ib** (thermal ellipsoids are given with 50% probability, and the hydrogen atoms of the Cp ligands are omitted).

the crystal of compound **Ia** are not evident. An example of a substantial nonequivalence of metal–metal bonds in tetrahedral cluster $[CrCp(\mu_3\text{-}O)]_4$ [29, 30] in which the Cr–Cr bonds differ by nearly 0.2 Å was described previously. Such a substantial violation of the expected symmetry T_d in the cluster is associated with its electronic structure (MO PMX calculations) and manifests magnetic properties (antiferromagnetism) [30, 31].

To obtain an additional information, we determined the structure of ruthenium cluster **I** in the crystal of its tetrahydrate **Ib**. Crystals of **Ib** (tetragonal crystal system, space group $I4_1/a$) have the composition $[Ru(\mu_3\text{-}CO)Cp]_4 \cdot 4(H_2O)$ (Fig. 2). The tetrahedral cluster in the crystal exists in the special position on the four-fold inversion axis; i.e., one ruthenium atom with the coordinated Cp ligand, one carbonyl ligand, and a solvate water molecule are crystallographically independent. Four Ru–Ru distances in the cluster are 2.7106(13) Å, and two distances are 2.7185(16) Å. The difference between these values is insignificant (lower than 0.01 Å), which agrees with the general symmetry of the cluster. The Ru–C(CO) distances (three independent values) remain slightly nonequivalent (Table 2), which likely corresponds to the violation of the cylindrical symmetry of the carbonyl group and an impossibility of binding equally to three metal atoms. Asymmetry of the carbonyl group coordination can also be due to the participation of the carbonyl O(1) oxygen atom in the formation of a hydrogen bond with the water molecule (hydrogen bond parameters are given in Table 3). In particular, the transoid arrangement of the oxygen O(1*w*) atom to the shortest Ru–C(CO) bond can be mentioned (torsion angle O(1*w*)...O(1)–C(1)–Ru(1) 168.8°).

In a crystal of **Ib**, the cluster molecule is surrounded by four water molecules, each of which forms the O(1)–H(1*wB*)...O(1) hydrogen bond with the oxygen atom of one of four carbonyl groups of cluster **I**. The second hydrogen atom H(1*wA*) is involved in the formation of the O(1*w*)–H(1*wA*)... $O(1w)_{0.75 + x, -1.25 - y, 0.25 + z}$ hydrogen bond with the adjacent water molecule to form an H-bonded screw chain of water molecules along the *c* axis of the crystal (Fig. 3b).

Note that, unlike carbonyl groups in organic compounds, carbonyl groups in transition metal complexes are prone to act as hydrogen bond acceptors to

Table 3. Hydrogen bond parameters in structure **Ib***

D–H...A	Distance, Å			Angle DHA, deg
	D–H	H...A	D...A	
O(1*w*)–H(1*w*A)...O(1*w*)[a]	0.98	1.75	2.716(10)	168
O(1*w*)–H(1*w*B)...O(1)	0.87	2.02	2.838(9)	156

* The position of the atom was revealed by the symmetry transform: [a] $-y + 5/4, x + 3/4, z - 1/4$.

a significantly lower extent. Nevertheless, the formation of hydrogen bonds O–H...OC–M involving the oxygen atoms of the metallocarbonyl groups was detected by IR spectroscopy in liquid xenon [32–34]. Structural confirmations of existence of similar interactions in crystals of metal carbonyl complexes are scarce. A close example was described for the crystal of tetrahydrate $[Tc(CO)_3(\mu_3\text{-}OH)]_4 \cdot 4(H_2O)$ [35]. In this crystal, the cubane cluster of technetium acts simultaneously as a donor (μ_3-OH ligands) and an acceptor (terminal metallocarbonyl groups) of hydrogen bonds toward the molecules of water of crystallization. The water molecules form a hydrogen-bonded tetramer instead of the screw chain as in the crystal of compound **Ib**.

The symmetry conditions for crystal **Ib** lead to equivalent intermolecular contacts for the external fragments of cluster **I**. All the four oxygen atoms of the carbonyl groups participate in the same hydrogen bonds with the water molecules, and each Cp ligand forms the same set of contacts with adjacent molecules. Among the latter, contacts corresponding to π–π stacking between parallel Cp rings of the adjacent molecules of cluster **I** can be distinguished (interplanar distance 3.17 Å, distance between ring centroids 4.18 Å, shortest interatomic distance $C(4)...C(4)_{1.5-x, 1.5-y, 0.5-z}$ 3.190(13) Å). In less symmetrical crystal of **Ia**, two independent Cp rings form different sets of intermolecular contacts (Fig. 3a). One of the Cp rings is involved in relatively weak π–π stacking with the parallel Cp ring of the adjacent cluster molecule (interplanar distance 3.67 Å, distance between ring centroids 4.72 Å, shortest interatomic distance $C(2)...C(2)_{0.5-x, 0.5-y, 1-z}$ 3.712(8) Å). The second symmetrically independent Cp ring participates only in weak C–H...π contacts, which are characterized by an approximately perpendicular arrangement of the adjacent rings.

Thus, in spite of specific intermolecular interactions involving oxygen atoms of the carbonyl groups (hydrogen bonds with water molecules) in crystal **Ib**, the structure of the cluster $Ru_4(CO)_4$ cage almost does not deviate from the ideal T_d symmetry and the averaged values of bonds of all types in cluster $[Ru(\mu_3\text{-}CO)Cp]_4$ coincide with their average values in crystal **Ia**. The more symmetrical structure of the cluster in tetrahydrate **Ib** is explained, most likely, by the symmetry of the crystal packing predetermining equivalence of intermolecular contacts in all directions. Nonequivalence of the crystalline environment in structure **Ia** even in the absence of intermolecular

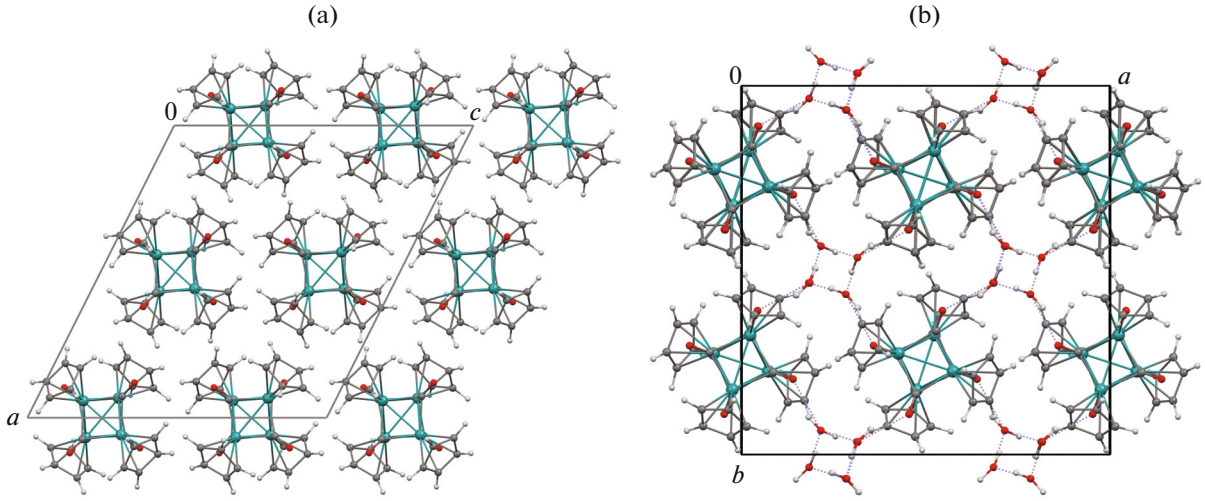

Fig. 3. Fragments of molecular packing in the crystal: (a) $[Ru(\mu_3\text{-}CO)Cp]_4$ (**Ia**) in the projection along the *b* axis of the crystal and (b) tetrahydrate $[Ru(\mu_3\text{-}CO)Cp]_4 \cdot 4(H_2O)$ (**Ib**) in the projection along the *c* axis of the crystal. Hydrogen bonds are shown by dash.

Table 4. Metal–metal bond lengths in selected ruthenium complexes with the number of metals from 2 to 4 and containing Cp, H, and CO ligands

Compound	Ru–Ru, Å	References
trans-$Ru_2(CO)_2(\mu\text{-}CO)_2(Cp)_2$	2.7412(4)	[36]
$Ru_3(CO)_{12}$	2.8459(4)–2.8558(4) ⟨2.850⟩	[37]
$Ru_3(CO)_3(\mu\text{-}H)_3(Cp)_3$	2.947(l)–2.954(1) ⟨2.950⟩	[38]
$Ru_4(\mu_3\text{-}CO)_2(\mu_3\text{-}CH)(\mu_3\text{-}H)(Cp)_4$	2.689(3)–2.727(4) ⟨2.712⟩	[39]
$Ru_4(\mu_3\text{-}H)_4(Cp)_2(Cp^*)_2$	2.7270(4)–2.7713(4) ⟨2.745⟩	[40]
$Ru_4(CO)_{12}(\mu\text{-}H)_4$	2.7839(8)–2.9565(7) ⟨2.895⟩	[41]
$Ru_4(\mu_3\text{-}CO)_4(Cp)_4$	2.6872(5)–2.7369(5) ⟨2.716⟩	This work
$Ru_4(\mu_3\text{-}CO)_4(Cp)_4\cdot 4(H_2O)$	2.7106(13)–2.7185(16) ⟨2.713⟩	This work

interactions leads to slight distortions of the cluster geometry.

As said above, the average Ru–Ru bond lengths in tetrahedral cluster $[Ru(\mu_3\text{-}CO)Cp]_4$ in structures **Ia** and **Ib** coincide and amount to 2.716 and 2.713 Å, respectively. It was of interest to compare these values with the available data on the Ru–Ru bond lengths in the series of related ruthenium compounds (Table 4) [36–41].

First, the Ru–Ru bonds in tetrahedral cluster **I** are appreciably shorter than the bonds in $Ru_3(CO)_{12}$ (average 2.850 Å [37]), which is often used as a standard object for comparison when describing the polynuclear ruthenium carbonyl clusters. It is most likely that the shortening of the Ru–Ru bonds in compound **I** is affected by the contraction effect of the μ_3-bridging carbonyl ligands and an increased positive charge on the ruthenium atoms, each of which is linked with the cyclopentadienyl ligand. At the same time, the influence of electron delocalization effects in the polynuclear cluster system cannot be excluded. For comparison, the Ru–Ru bond length in the *trans*-$Ru_2(CO)_2(\mu\text{-}CO)_2(Cp)_2$ dimer is 2.7412(4) [36]. It should be mentioned that dimer $[Ru(CO)_2(Cp)]_2$ has several isomeric forms depending on the *cis*- or *trans*-arrangement of the Cp ligands and the presence or absence of bridging CO ligands in which the Ru–Ru bond length can vary in a broad range of 2.70–2.82 Å [3]. The Ru–Ru bonds are substantially elongated being 2.950 Å on the average in triruthenium complex $Ru_3(CO)_3(\mu\text{-}H)_3(Cp)_3$ containing three symmetrical bridging hydride ligands along with three cyclopentadienyl and three terminal carbonyl ligands [38].

Almost no compounds simultaneously containing Cp and CO ligands are observed among various tetrahedral ruthenium clusters (according to the Cambridge Structural Database (CSD) [42], 174 compounds were structurally characterized). The single similar $Ru_4(\mu_3\text{-}CO)_2(\mu_3\text{-}CH)(\mu_3\text{-}H)(Cp)_4$ cluster [39] also contains the μ_3-methylidine and μ_3-hydride ligands. In this cluster, the Ru–Ru bond lengths coincide in fact with the range of values for compound **I** (Table 4). Tetrahedral ruthenium clusters with cyclopentadienyl ligands are presented in the CSD mainly as polyhydride derivatives with the number of hydride ligands from 4 to 8 [40, 43, 44]. In the most symmetrical cluster $Ru_4(\mu_3\text{-}H)_4(Cp^{Et})_4$ (where $Cp^{Et} = C_5EtMe_4$) with four μ_3-bridging hydride ligands, the Ru–Ru bonds have approximately the same lengths: 2.7868(3)–2.7941(3) Å (average 2.790 Å). An increase in the number of hydride ligands leads to a decrease in the symmetry of the metal cage and cluster structure loosening with an increase in the Ru–Ru bond lengths to 2.918, 2.884, and 2.897 Å on the average for the clusters with 8, 7, and 6 hydride ligands, respectively [43].

Although tetrahedral ruthenium carbonyl cluster $Ru_4(CO)_{14}$ refers to clusters with the filled 18e shell for each metal atom according to the effective atomic number (EAN) rule, the cluster has not been described so far. There is a single report on the mass spectral detection of the $[Ru_4(CO)_{14}]^+$ cation in the gas phase [45]. The isoelectronic osmium analog $Os_4(CO)_{14}$ was prepared, and its crystal structure is known [46]. Diverse polyhydride derivatives $Ru_4(CO)_{13}(\mu\text{-}H)_2$ [47], $[Ru_4(CO)_{12}(\mu\text{-}H)_3]^-$ [48], and

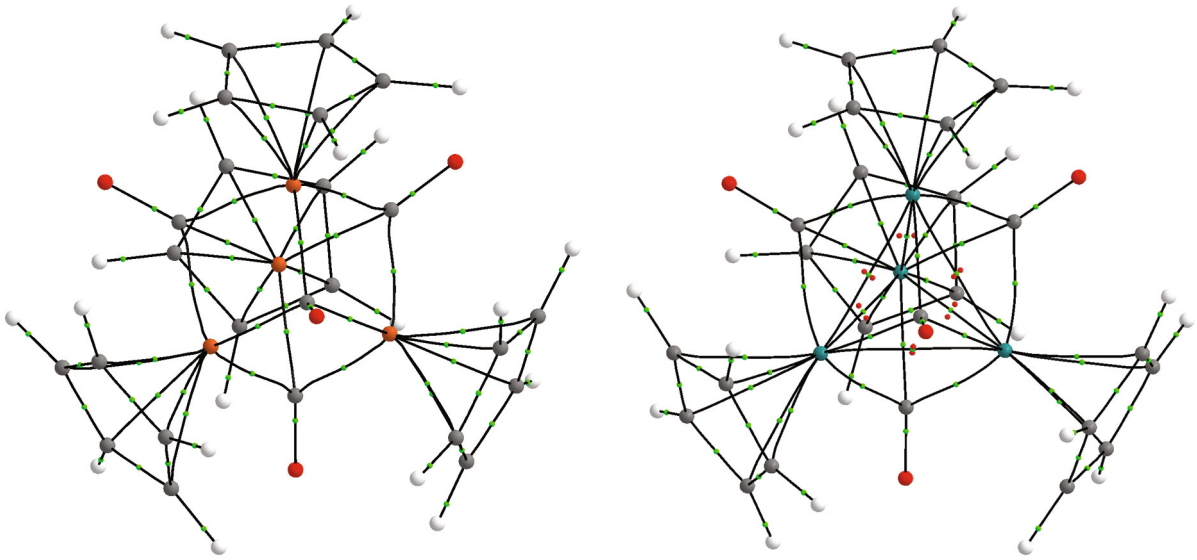

Fig. 4. Connectivity graphs of atoms in the isolated molecules $Fe_4(\mu_3\text{-}CO)_4(Cp)_4$ (left) and $Ru_4(\mu_3\text{-}CO)_4(Cp)_4$ (right) according to the data of topological analysis of the electron density. Green dots correspond to the critical points (3, −1). Selected critical points (3, +1) for the ruthenium complex are shown by red.

$Ru_4(CO)_{12}(\mu\text{-}H)_4$ [41] in which metal–metal bond lengths can vary in wide ranges depending on the position of the bridging hydride ligands are well known and structurally characterized (Table 4).

Based on the geometric considerations and results of literature analysis, we can assume that a combination of the tetrahedral symmetry with bridging carbonyl ligands makes the metal cage in $Ru_4(\mu_3\text{-}CO)_4(Cp)_4$ to be one of the strongest in this class of compounds (its Ru–Ru distance is one of the shortest among the considered analogs). However, this contradicts the experimental data for **Ia** and **Ib**: the influence of the crystal packing on the geometry of the compound is very substantial, although the average distance between the metal atoms is retained. Remind that a similar structural nonrigidity of the molecule does not appear, in fact, for similar iron compound $Fe_4(\mu_3\text{-}CO)_4(Cp)_4$ [28]: the crystal field is not sufficient to distort the metal cage structure in the crystal of the pure substance (Fe–Fe 2.507–2.529 Å). The study of these features was supplemented by the data of quantum-chemical calculations of isolated molecules of $Fe_4(\mu_3\text{-}CO)_4(Cp)_4$ (**I-Fe**) and $Ru_4(\mu_3\text{-}CO)_4(Cp)_4$ (**I-Ru**) using a topological analysis of the electron density [49], which makes it possible to reveal all so-called binding interactions and also to evaluate their strength with respect to both the bond energy and rigidity.

Geometry optimization of both isolated molecules results in the symmetrical configuration even when completely ignoring the symmetry of the electron integrals in the calculation: Fe–Fe 2.523–2.545 Å and Ru–Ru 2.695–2.696 Å. The chosen calculation method (PBE0-D3/def2TZVP combined with the pseudopotentials for the description of core electrons and ignoring solvation effects) rather well reproduced the geometry of the molecules in the crystal: the root-mean-square deviations for the non-hydrogen atoms were only 0.09 and 0.12 Å for **I-Fe** and **I-Ru**, respectively. This confirms the hypothesis about crystal packing effects as a single factor predetermining fine features of the metal cage of the ruthenium cluster in structure **Ia**.

The energy of interactions of the metal atom turns out to be higher for the ruthenium compound, which is well consistent with the concepts on a higher strength of interactions of the 5*d*-metal atom in the clusters. For example, the transition from the $M_4(\mu_3\text{-}CO)_4(Cp)_4$ structures to model systems corresponding to the hypothetical dissociation of the complexes into the CpM and Co fragments with the removal of these fragments from the center of gravity at 40 Å without geometry optimization is less energy expensive for the iron compound (145.9 kcal mol^{-1} per metal atom vs. 187.6 kcal mol^{-1} for the ruthenium analog). This is confirmed, to some extent, by the results of topological analysis of the electron density function $\rho(\mathbf{r})$. Here it is important that the connectivity graphs of atoms for **I-Fe** and **I-Ru** differ: according to the data of topological analysis of $\rho(\mathbf{r})$, **I-Ru** contains metal–metal bonds, whereas no these interactions are observed in **I-Fe** (Fig. 4).

According to the data of the Espinosa–Molins–Lecomte correlation scheme [50–52], which analyzes the density of the potential energy of electrons at the critical points (3, −1) of the $\rho(\mathbf{r})$ function, the average energy of all binding interactions of the metal atom in

I-Ru is 359.6 kcal mol^{-1}, whereas a similar value for the iron complex is 338.1 kcal mol^{-1} only. A detailed analysis of the contributions showed that the average energy of binding interactions of the CpM fragments with each other and with carbonyl ligands was 150 and 173 kcal mol^{-1} for the iron and ruthenium complexes, respectively, which rather well describes the model dissociation energy of the $M_4(Cp)_4(\mu_3\text{-}CO)_4$ molecules into the CpM and CO fragments (see above). The energies of interactions of the metal atoms with the carbonyl ligands are near equal (145 and 150 kcal mol^{-1} for M = Ru and M = Fe, respectively), and the difference in dissociation energies is determined by the presence of interactions between the metal atoms. Note that this correlation scheme has already been applied for the estimation of the metal–ligand energy [53–55].

Thus, the estimation of the energy of interactions of the ruthenium atoms does not allow one to explain the observed nonrigidity of the metal cage in structures **Ia** and **Ib**. At the same time, the calculation of normal vibration frequencies for **I-Fe** and **I-Ru** expectedly shows that a change in the metal cage geometry in both clusters corresponds to the so-called soft modes (wavenumbers lower than 600 cm^{-1}), i.e., is characterized by a slope potential energy surface. When comparing the strength of interatomic interactions with this dynamics, it is necessary to take into account that the potential minimum depth already must not correlate with its width and a correct description of vibrational processes requires applying anharmonic corrections. In other words, the rigidity of interactions of the metal atom must not be higher for the system with a higher energy of interactions of the metal atom.

In fact, the estimation of effective force constants of binding interactions of the metal atom using the correlation scheme that examines the density integrals of the potential energy of electrons weighed to internuclear distances over the interatomic surfaces [56] shows that the metal cage structure is less rigid in the ruthenium complex. For instance, the average value of the sum of weighed surface integrals for the metal atom in **I-Ru** is –1.19 au, whereas a similar metrics for the iron complex is –1.28 au. This is consistent with the results of analysis of normal vibration coordinates: the highest wavenumber of the vibration that significantly changes the coordinates of the metal atoms (more than by 0.016 Å for the normal coordinate) is 513 cm^{-1} for the ruthenium complex and 613 cm^{-1} for the iron complex. At the same time, the average sums of weighed integrals of the potential energy density describing the rigidity of interactions of the CpM fragment with the environment are very close for two compounds and are only slightly lower by absolute value for the ruthenium analog (–0.76 against –0.78 au for the iron compound). Thus, the interactions with the cyclopentadienyl rings contribute mainly to the difference in rigidities of the metal atom polyhedron. Interestingly, the rigidity of the metal–carbonyl interactions is lower for $Ru_4(Cp)_4(\mu_3\text{-}CO)_4$ (–0.74 against –0.78 au for the iron compounds), which is compensated by the contributions to the rigidity of the ruthenium polyhedron from the metal–metal interactions (–0.02 au). Note that a lower rigidity of the Ru–Ru bonds in $Ru_4(Cp)_4(\mu_3\text{-}CO)_4$ is well consistent with both classical concepts (significant overlapping of atomic orbitals should change weakly with a change in the distance between the atomic centers) and specific features of the topology of $\rho(\mathbf{r})$: the critical points (3, –1) corresponding to the Ru–Ru bond are rather close to the critical points (3, +1), which allows one to expect their degeneracy and respective variation of the connectivity graph at any sufficiently small parameter wiggling (vibrational shifts of nuclei) [57].

To conclude, the thermal reaction of cyclopentadiene with $Ru_3(CO)_{12}$ affords a multicomponent mixture of the products, among which ruthenocene and tetranuclear cluster $[Ru(\mu_3\text{-}CO)Cp]_4$ were identified in minor amounts along with the usually isolated $[Ru(CO)_2Cp]_2$ ruthenium dimer. The formation of the tetranuclear cluster confirms the general tendency of ruthenium carbonyls to form polynuclear cluster compounds. The structure of cluster $[Ru(\mu_3\text{-}CO)Cp]_4$ was first determined by the single-crystal XRD data for the pure compound and its tetrahydrate. The distortion of the cubane cage of $Ru_4(CO)_4$ from the ideal T_d symmetry observed in the crystal is predetermined by anisotropy of the crystalline environment. According to the theoretical calculations, the changes in the metal cage structure cannot be explained from the viewpoint of energetics of interatomic interactions: they are a consequence of the slope character of the potential energy surface provided by their lower rigidity. This again puts a question about a necessity of systematic analysis of metrics of the chemical bond strength during structural chemical studies [58].

ACKNOWLEDGMENTS

The authors are grateful to D.V. Muratov for help in discussion of the results and to A.S. Peregudov for recording NMR spectra. The XRD studies were carried out using the equipment of the JRC PMR IGIC RAS.

FUNDING

This work was carried out in the framework of the state assignment no. 075-03-2023-642 (Nesmeyanov Institute of Organoelement Compounds, Russian Academy of Sciences) by the Ministry of Science and Higher Education of the Russian Federation. The theoretical part of the work was supported by the Ministry of Science and Higher Education of the Russian Federation as a part of the state assignment of the Kurnakov Institute of General and Inorganic Chemistry (Russian Academy of Sciences).

CONFLICT OF INTEREST

The authors of this work declare that they have no conflicts of interest.

REFERENCES

1. Jaworska, M., Macyk, W., and Stasicka, Z., *Struct. Bond*, 2004, vol. 106, p. 153.
2. Anna, J.M., King, J.T., and Kubarych, K.J., *Inorg. Chem.*, 2011, vol. 50, p. 9273.
3. Bitterwolf, T.E., *Coord. Chem. Rev.*, 2000, vols. 206–207, p. 419.
4. Bennett, M.A., Bruce, M.I., and Matheson, T.W., in *Comprehensive Organometallic Chemistry*, Wilkinson, G., Stone, F.G.A., and Abel, E.W., Eds., Oxford: Pergamon, 1982, vol. 4, p. 821.
5. Haines, R.J., in *Comprehensive Organometallic Chemistry II*, Abel, E.W., Stone, F.G.A., and Wilkinson, G., Eds., Oxford: Pergamon, 1995, vol. 7, p. 625.
6. Osintseva, S.V., Dolgushin, F.M., Shtel'tser, N.A., et al., *Organometallics*, 2010, vol. 29, p. 1012.
7. Osintseva, S.V., Shtel'tser, N.A., Peregudov, A.S., et al., *Polyhedron*, 2018, vol. 148, p. 147.
8. Humphries, A.P. and Knox, S.A.R., *J. Chem. Soc., Chem. Commun.*, 1973, p. 326.
9. Humphries, A.P. and Knox, S.A.R., *J. Chem. Soc., Dalton Trans.*, 1975, p. 1710.
10. Doherty, N.M., Knox, S.A.R., Morris, M.J., et al., *Inorganic Syntheses: Reagents for Transition Metal Complex and Organometallic Syntheses*, 1990, vol. 28, p. 189.
11. Kalz, K.F., Kindermann, N., Sheng-Qi Xiang, et al., *Organometallics*, 2014, vol. 33, p. 1475.
12. Pomeroy, R.K., in *Comprehensive Organometallic Chemistry II*, Abel, E.W., Stone, F.G.A., and Wilkinson, G., Eds., Oxford: Pergamon, 1995, vol. 7, p. 835.
13. Davison, A., McCleverty, J.A., and Wilkinson, G., *J. Chem. Soc.*, 1963, p. 1133.
14. Fischer, R.D., Vogler, A., and Noack, K., *J. Organomet. Chem.*, 1967, vol. 7, p. 135.
15. Wilkinson, G., *J. Am. Chem. Soc.*, 1952, vol. 74, p. 6146.
16. Haines, R.J. and Preez, A.L., *J. Chem. Soc., Dalton Trans.*, 1972, p. 945.
17. Blackmore, T., Cotton, J.D., Bruce, M.I., and Stone, F.G.A., *J. Chem. Soc. A*, 1968, p. 2932.
18. Knox, S.A.R. and Morris, M.J., *J. Chem. Soc., Dalton Trans.*, 1987, p. 2087.
19. Sheldrick, G.M., *SADABS*, Madison: Bruker AXS Inc., 1997.
20. Sheldrick, G.M., *Acta Crystallogr., Sect. C: Struct. Chem.*, 2015, vol. 71, p. 3.
21. Frisch, M.J., Trucks, G.W., Schlegel, H.B., et al., *Gaussian 09. Revision D.01*, Wallingford: Gaussian, Inc., 2016.
22. Perdew, J., Ernzerhof, M., and Burke, K., *J. Chem. Phys.*, 1996, vol. 105, p. 9982.
23. Weigend, F., *Phys. Chem. Chem. Phys.*, 2006, vol. 8, p. 1057.
24. Grimme, S., Antony, J., Ehrlich, S., and Krieg, H., *J. Chem. Phys.*, 2010, vol. 132, p. 154104.
25. Grimme, S., Ehrlich, S., and Goerigk, L., *J. Comput. Chem.*, 2011, vol. 32, p. 1456.
26. Keith, T., *AIMAll (version 19.10.12). TK Gristmill Software*, Overland Park KS, 2019 (aim.tkgristmill.com).
27. Feasey, N.D., Forrow, N.J., Hogarth, G., et al., *J. Organomet. Chem.*, 1984, vol. 267, p. C41.
28. Neuman, M.A., Trinh-Toan, and Dahl, L.F., *J. Am. Chem. Soc.*, 1972, vol. 94, p. 3383.
29. Bottomley, F., Paez, D.E., and White, P.S., *J. Am. Chem. Soc.*, 1982, vol. 104, p. 5651.
30. Eremenko, I.L., Nefedov, S.E., and Pasynskii, A.A., *J. Organomet. Chem.*, 1989, vol. 368, p. 185.
31. Bottomley, F. and Grein, F., *Inorg. Chem.*, 1982, vol. 21, p. 4170.
32. Lokshin, B.V., Kazaryan, S.G., and Ginzburg, A.G., *Russ. Chem. Bull.*, 1986, vol. 35, p. 2390.
33. Lokshin, B.V., Kazaryan, S.G., and Ginzburg, A.G., *J. Mol. Struct.*, 1988, vol. 174, p. 29.
34. Hamley, P.A., Kazarian, S.G., and Poliakoff, M., *Organometallics*, 1994, vol. 13, no. 5, p. 1767.
35. Zuhayra, M., Kampen, W.U., Henze, E., et al., *J. Am. Chem. Soc.*, 2006, vol. 128, no. 2, p. 424.
36. Straub, T., Haukka, M., and Pakkanen, T.A., *J. Organomet. Chem.*, 2000, vol. 612, p. 106.
37. Gervasio, G., Marabello, D., Bianchi, R., and Forni, A., *J. Phys. Chem. A*, 2010, vol. 114, p. 9368.
38. Forrow, N.J., Knox, S.A.R., Morris, M.J., and Orpen, A.G., *J. Chem. Soc., Chem. Commun.*, 1983, p. 234.
39. Akita, M., Hua, R., Nakanishi, S., et al., *Organometallics*, 1997, vol. 16, p. 5572.
40. Kameo, H., Sakaki, S., Ohki, Y., et al., *Inorg. Chem.*, 2021, vol. 60, no. 3, p. 1550.
41. Wilson, R.D., Wu, S.M., Love, R.A., and Bau, R., *Inorg. Chem.*, 1978, vol. 17, no. 5, p. 1271.
42. Groom, C.R., Bruno, I.J., Lightfoot, M.P., and Ward, S.C., *Acta Crystallogr., Sect. B: Struct. Sci., Cryst. Eng. Mater.*, 2016, vol. 72, p. 171.
43. Kameo, H., Ito, Y., Shimogawa, R., Koizumi, A., et al., *Dalton Trans.*, 2017, vol. 46, p. 5631.
44. Ohki, Y., Uehara, N., and Suzuki, H., *Angew. Chem., Int. Ed. Engl.*, 2002, vol. 41, no. 21, p. 4085.
45. Lang, S.M., Förtig, S.U., Bernhardt, T.M., et al., *J. Phys. Chem. A*, 2014, vol. 118, p. 8356.
46. Johnston, V.J., Einstein, F.W.B., and Pomeroy, R.K., *Organometallics*, 1988, vol. 7, p. 1867.
47. Rheingold, A.L., Haggerty, B.S., Geoffroy, G.L., and Han, S.-H., *J. Organomet. Chem.*, 1990, vol. 384, p. 209.
48. McPartlin, M. and Nelson, W.J.H., *J. Chem. Soc., Dalton Trans.*, 1986, p. 1557.
49. Matta, C.F. and Boyd, R.J., *The Quantum Theory of Atoms in Molecules: From Solid State to DNA and Drug Design*, Weinheim: Wiley-VCH, 2007.
50. Espinosa, E., Molins, E., and Lecomte, C., *Chem. Phys. Lett.*, 1998, vol. 285, p. 170.
51. Romanova, A.A., Lyssenko, K.A., and Ananyev, I.V., *J. Comput. Chem.*, 2018, vol. 39, p. 1607.
52. Lyssenko, K., *Mendeleev Commun.*, 2012, vol. 22, p. 1.

53. Borissova, A.O., Korlyukov, A.A., Antipin, M.Yu., and Lyssenko, K.A., *J. Phys. Chem. A*, 2008, vol. 112, p. 11519.

54. Ananyev, I.V., Nefedov, S.E., and Lyssenko, K.A., *Eur. J. Inorg. Chem.*, 2013, vol. 2013, p. 2736.

55. Puntus, L.N., Lyssenko, K.A., Antipin, M.Yu., and Buenzli, J.-C.G., *Inorg. Chem.*, 2008, vol. 47, p. 11095.

56. Ananyev, I.V., Karnoukhova, V.A., Dmitrienko, A.O., and Lyssenko, K.A., *J. Phys. Chem. A*, 2017, vol. 121, p. 4517.

57. Ananyev, I.V., Medvedev, M.G., Aldoshin, S.M., et al., *Russ. Chem. Bull*, 2016, vol. 65, p. 1473.

58. Cremer, D., Wu, A., Larsson, A., and Kraka, E., *J. Mol. Model*, 2000, vol. 6, p. 396.

Translated by E. Yablonskaya